

Article

Assessment of Radiometric Resolution Impact on Remote Sensing Data Classification Accuracy

Natalia Verde ^{1,*} , Giorgos Mallinis ^{1,2} , Maria Tsakiri-Strati ¹, Charalampos Georgiadis ³ and Petros Patias ¹ 

¹ Laboratory of Photogrammetry and Remote Sensing, Department of Cadastre, Photogrammetry and Cartography, Faculty of Rural and Surveying Engineering, Aristotle University of Thessaloniki, 54124 Thessaloniki, Greece; gmallin@fmenr.duth.gr (G.M.); martsaki@topo.auth.gr (M.T.-S.); patias@auth.gr (P.P.)

² Laboratory of Forest Remote Sensing, Department of Forestry and Management of the Environment and Natural Resources, Democritus University of Thrace, 68200 Orestiada, Greece

³ School Civil Engineering, Aristotle University of Thessaloniki, 54124 Thessaloniki, Greece; harrisg@civil.auth.gr

* Correspondence: nverde@topo.auth.gr; Tel.: +30-2310-99-6116

Received: 27 June 2018; Accepted: 9 August 2018; Published: 11 August 2018



Abstract: Improved sensor characteristics are generally assumed to increase the potential accuracy of image classification and information extraction from remote sensing imagery. However, the increase in data volume caused by these improvements raise challenges associated with the selection, storage, and processing of this data, and with the cost-effective and timely analysis of the remote sensing datasets. Previous research has extensively assessed the relevance and impact of spatial, spectral and temporal resolution of satellite data on classification accuracy, but little attention has been given to the impact of radiometric resolution. This study focuses on the role of radiometric resolution on classification accuracy of remote sensing data through different classification experiments over three different sites. The experiments were carried out using fine and low scale radiometric resolution images classified through a bagging classification tree. The classification experiments addressed different aspects of the classification road map, including among others, binary and multiclass classification schemes, spectrally and spatially enhanced images, as well as pixel and objects as units of the classification. In addition, the impact of image radiometric resolution on computational time and the information content in fine- and low-resolution images was also explored. While in certain cases, higher radiometric resolution has led to up to 8% higher classification accuracies compared to lower resolution radiometric data, other results indicate that higher radiometric resolution does not necessarily imply improved classification accuracy. Also, classification accuracy of spectral indices and texture bands is not related so much to the radiometric resolution of the original remote sensing images but rather to their own radiometric resolution. Overall, the results of this study suggest that data selection and classification need not always adhere to the highest possible radiometric resolution.

Keywords: radiometric resolution; indices; texture; object-based; multispectral; bagging classification tree; entropy

1. Introduction

In recent years, the improvements in spatial, spectral, radiometric, and temporal resolution of remote sensing imagery data has led to increased interest in the scientific community, as well as among end users in employing remote sensing data to new applications and operational needs.

However, as resolution increases, the complexity of data also increases and in order to fully exploit the potential of the new generation of remote sensing computers and sensors, a number of

challenges need to be addressed. Improvement of resolution also results in high data volumes and storage issues [1]. With regard to storage requirements for example, NASA's Earth Observing System Data and Information System (EOSDIS) has an extensive archive of remote sensing data currently exceeding 7.5 petabytes, with their data undergoing a growth of 4 TB daily [2]. These huge data volumes require the usage of image compression techniques, providing either 'lossless' compression or 'lossy' compression [3]. Furthermore, the majority of traditional image processing algorithms fail when the data resolution is greatly increased and it is often necessary to create new processing algorithms [4].

Radiometric resolution refers to the number of bit depth divisions, associated also with the sensitivity of the sensor to incoming reflectance [1]. It is a combination of two components related to the design and operation of sensor systems. The first component is sensor system noise and the second is the number of quantizing levels present in the analogue to digital converter of the sensor system [5].

Radiometric resolution has also witnessed some major improvements along the course of remote sensing evolution. While the first optical satellite systems that were developed used sensors with a 6-bit radiometric resolution (Landsat multispectral scanner sensors), over the years, along with the development of technology, radiometry of sensors also improved, resulting in products of up to 14 bits (KOMPSAT 3 satellite sensor).

The potential benefits of higher radiometry of satellite data have only been partially examined in literature [6]. The first studies conducted on the effect of radiometric resolution on image information were focused on the comparison of 8-bit data from the Thematic Mapper (TM) sensor with 6-bit data from the multispectral scanner system (MSS) sensor, of the Landsat-4 satellite. Tucker [5], was the first who studied the relationship between radiometric resolution and the ability to distinguish vegetation in 256-level (8 bits) TM and 64-level (6 bits) MSS images. The study came to the conclusion that there was an overall improvement of only 2–3% in the TM image. Irons et al. [7], also examined the effect of radiometric resolution of actual and degraded TM data, on pixel-based maximum likelihood classification, while keeping constant spatial and spectral resolution. The study found increases of overall accuracies up to 8% in the 8-bit data over the degraded 6-bit data.

During the next years, the emerge of hyperspectral imagery led to studies which compared hyperspectral data of higher radiometric resolution with artificially simulated data of same-type sensors, by degrading their radiometric resolution. The results indicated that images with higher radiometry had an improved accuracy of 0.8–6% [8,9]. Singh et al. [10], assessed also spatial, temporal and radiometric resolution impact by comparing NDVI-based classification results. Other researchers identified that, spectral resolution is more important than spatial or radiometric resolution to improve classification accuracy [8].

In a study devoted entirely to radiometric resolution, Rama Rao et al. [11], also found that overall classification accuracy of higher radiometry data over an agricultural area, increased by only 3%. In a similar study, Rao et al. [6], demonstrated that using 12-bit instead of 7-bit data for Leaf Area Index (LAI) computation using the Normalized Difference Vegetation Index (NDVI), had a marginal increase in the accuracy (1–2%).

Along with the investigation of radiometric resolution impact on image classification accuracy, other studies assessed the radiometric resolution impact by comparing the amount of information contained in a high radiometry image against a lower radiometry image. Bernstein et al. [12], were the first to use a measure known as entropy to compare the amount of information (in bits/pixel) for 8-bit and 6-bit images from the TM and MSS Landsat-4 sensors. The analysis proved the higher information content in the TM sensor data (1–2 bits/pixel). Entropy was also used in a study by Malila [13], but in the form of relative entropy, to measure the information content in the TM and MSS sensor bands and the corresponding Tasseled Cap (TC) transformed bands. Similar studies, such as those of Masek et al. [14], and Karnieli et al. [15], which, compared the amount of information between images with the same radiometry using entropy, indicated that the Landsat-7 ETM+ sensor data contained more information than the Landsat-5 TM sensor data, despite having the same 8-bit radiometric resolution. The effect of radiometry was examined through multifractal analysis and

entropy in a study by Alonso et al. [16]. The results demonstrated a greater influence of radiometric resolution on blue and green bands than on red and near infrared ones.

Adopting a different approach, Elmore & Mustard [17], compared the percentage of green coverage resulting from data of different radiometric resolutions, over the same study area, demonstrating that the 12-bit EO-1 ALI data had a standard deviation of an estimated green percentage slightly lower ($\pm 5.61\%$) from the 8-bit ETM+ data ($\pm 6.15\%$). Finally, using a different approach Orych et al. [18], investigated the impact of radiometric resolution on multispectral video cameras, using laboratory reference data, coming from a spectroradiometer. The video camera with the higher radiometric resolution showed a slight improvement in accuracy.

From the aforementioned studies, it can be noticed that little attention has been given in the literature to the impact of radiometric resolution in the information extraction process from remote sensing images. On the contrary, extensive studies have been conducted on the relevance and impact of spatial [7,19,20] and spectral resolution [21,22] of remote sensing data in terms of classification accuracy and information extraction potential. In addition, the existing studies dealing with radiometric resolution are implemented in a specific site and a single variable of interest (i.e., LAI or fractional vegetation or single land use/land cover classification). Therefore, within this study we attempt to expand previous research on the impact of radiometric resolution on information extraction from remote sensing imagery. We evaluate its impact on classification experiments over three different landscapes (peri-urban, forest and agricultural), with different sensors and classification schemes, as well as different units of analysis (pixel-object), original and synthetic bands and temporal resolutions. The classification experiments are implemented using a bagging tree classifier requiring minimum user-defined parameters while being capable of handling small sample sizes [23]. The relevance of the study becomes more profound considering the impact of the radiometric resolution on data volume and associated storage and processing capacity required for handling the finer spatial and temporal resolution images available nowadays.

The overall research goal of this study is to assess the impact of radiometric resolution on the classification of remote sensing data. More specifically, the impact of radiometry on accuracy was assessed using (a) single date very high spatial resolution, under binary and multiclass schemes (b) bitemporal change detection (c) texture-based classification and (d) per-field multiseasonal classification using original and synthetic bands (spectral indices). Finally, the impact of image radiometry is also assessed in terms of changes in entropy information as well, in terms of computational cost.

2. Materials and Methods

2.1. Study Sites and Satellite Data

Three study sites with diverse scene characteristics were selected over Northern Greece. The first study site was in the district of Triadi, located in the eastern part of the rural-urban fringes of Thessaloniki city—Greece's second major economic, industrial, commercial and political center. Triadi has experienced some dense construction activity in recent years, having a building stock consisting mainly of single-family houses, with clay tile roofs, in a multitude of shapes and profiles. The remote sensing data used over the 96 hectares site, consists of a pair of Ikonos-2 images acquired on September 2007 and on March 2010. Both images were recorded in an 11-bit radiometric resolution range and were already pansharpened to 1-m spatial resolution (Figure 1).

The second study site was the Aristotle's University Forest, in the mountainous areas of Chalkidiki Prefecture that covers an area of 445 ha. The altitude ranges from 320 to 1200 m and the forest species of the area include Italian oak, European black pine, beech, and Calabrian pine. Also, patches within the area are covered with shrubs and low herbaceous vegetation. An 11-bit radiometric resolution Quickbird bundle (multispectral and panchromatic) satellite image, acquired on June 2004 was the primary source of information for the classification experiments over this site.

The third study site was located within the Axios rural area, in the western part of the Thessaloniki Prefecture. The site extends across approximately 3400 ha and its topography is characterized as almost perfectly flat. It is an agricultural area with complex cultivation patterns dominated by rice and cotton while maize and lucerne crops are planted to a smaller extent. A set of five Sentinel-2 images acquired on 2017 were employed for crop classification in the third site. The Sentinel-2 MSI sensor, records 13 spectral bands in the visible, near-infrared, and short-wave infrared parts of the spectrum, with a spatial resolution up to 10 m, having 12-bit radiometric resolution [24]. Sentinel-2 data processed at level-2A was used. This product level provides Bottom Of Atmosphere (BOA) reflectance images, in cartographic geometry (UTM/WGS84 projection) [25]. The images of the temporal sequence were acquired between March and August considering local crop phenological cycle [26].

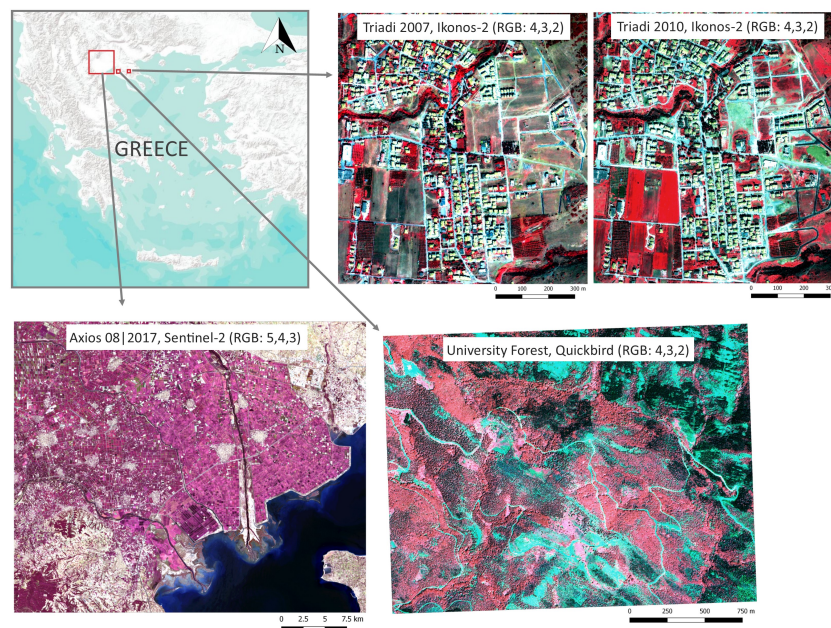


Figure 1. Location of the three experimental sites and false color compositions of the satellite images used in the analysis.

2.2. Bagging Classification Trees

Bagging classification trees (BCT) is a supervised nonparametric ensemble learning algorithm that fits a number of decision tree classifiers on various subsamples of the dataset and uses averaging to improve the predictive accuracy and control overfitting [27]. In terms of image classification, BCT does not require any knowledge about data statistical distribution, driven by the relationship between independent and dependent variables and has a small execution time compared to other classification methods. Furthermore, requirements in terms of training sample size needed in a BCT classification are fairly small compared to other algorithms [28]. Out of this sample, two-thirds are used for training the model, with the remaining one third (out-of-the bag samples) used in an internal cross-validation technique for model validation. This error estimate is known as the out-of-bag (OOB) error [28]. In the present study, the BCT classifier was implemented using the 'randomForest' package [29], within the R environment software [30]. Important parameters that must be specified for implementation of the BCT algorithm are (a) the number of input variables randomly chosen at each split (M_{try}), (b) the number of trees in the forest (N_{tree}), and (c) the node size, which allows specification of the minimum number of observations in a node [31]. The number of trees grown (N_{tree}) for each classification was set to the default value of 500, as it is the most commonly used value in the majority of studies [28], while the optimal number of random variables to be tested in each tree (M_{try}) was set equal to the number of variables available for

each classification, forcing the algorithm to implement a BCT and use all the bands in order to avoid the ‘randomness’ of developing different models each time and minimize the influence of the spectral component in the classification accuracy. The minimal size of the terminal nodes of the trees (nodesize) was set to 1, the default value of the ‘randomForest’ package for classification.

2.3. Accuracy Assessment

To assess the relationship of radiometric resolution and classification accuracy, the out-of-bag (OOB) rate for each classification was calculated. Furthermore, confusion matrices were derived from independent validation samples selected through stratified random sampling within each study site. The ‘kappa hat’ (khat) statistic and the overall accuracy (OA), were derived from the matrices to quantify the performance of BCT classifications and the contribution of radiometric resolution to classification accuracy. The khat is computed according to the following formula [32]:

$$\text{Khat} = \frac{N \sum_{i=1}^k N_{ii} - \sum_{i=1}^k (N_{i+} * N_{+i})}{N^2 - \sum_{i=1}^k (N_{i+} * N_{+i})}, \quad (1)$$

where k is the number of rows in the matrix, N_{ij} is the number of observations in row i and column j , N_{i+} and N_{+i} are the marginal totals of row i and column i , respectively, and N is the total number of observations. The khat is an attractive index of classification accuracy, as it allows the comparison of different confusion matrices, and so, different classifications [33].

2.4. Image Entropy

Entropy is a measure of ‘disorder’ of data and has been adopted in remote sensing either in the form of texture measure, maximizing the common information in a neighborhood [34], or as an absolute measurement, used to evaluate and compare the information content of different systems based on image histogram frequencies [35]. In mathematic terms, entropy of an image is defined as:

$$H = - \sum_{i=0}^n p(i) * \log_2 p(i), \quad (2)$$

where $p(i)$ gives the probability of occurrence of a specific pixel value i in the image, and n the number of bins in the image histogram (image bits).

In this study, entropy of each band was calculated based on the frequency histogram for the different radiometric resolution images. Calculations were done with an R script. In R’s ‘entropy’ package [36], entropy is calculated in several ways, including the frequency histogram, which is the most simple and widespread approach. In R, this method is referred to as the ‘maximum-likelihood’ (ML) method.

2.5. Design of the Experiments

Three different experiments were designed in order to assess linkages between classification accuracy and radiometric resolution under different classification schemes, spatial resolution, units of classification and image variables (Figure 2): (i) assessment of the radiometric resolution impact on the classification accuracy and change identification under a binary classification scheme and different spatial resolution, using two images acquired over the same area over a three-year period (experimental setting 1); (ii) assessment of the radiometric resolution impact in a multiclass classification problem employing spectral and texture features (experimental setting 2); (iii) assessment of the radiometric resolution impact on multiseasonal original and synthetic (spectral indices) band classification using a per-field classification approach (experimental setting 3). In all three experiments, images were rescaled from 16-bit to 8-bit radiometric resolution, using the linear rescale method [8,16,37], in order to artificially create the new images to study radiometric resolution effect on classification accuracy. Finally, in each experimental setting the same reference data samples were used for both high and low

radiometric resolution datasets while the processing time was also measured. All classification scripts were ran on a 64-bit system, with a quad-core Intel Core i7 920 processor, at 2.6 GHz and 24 GB RAM.

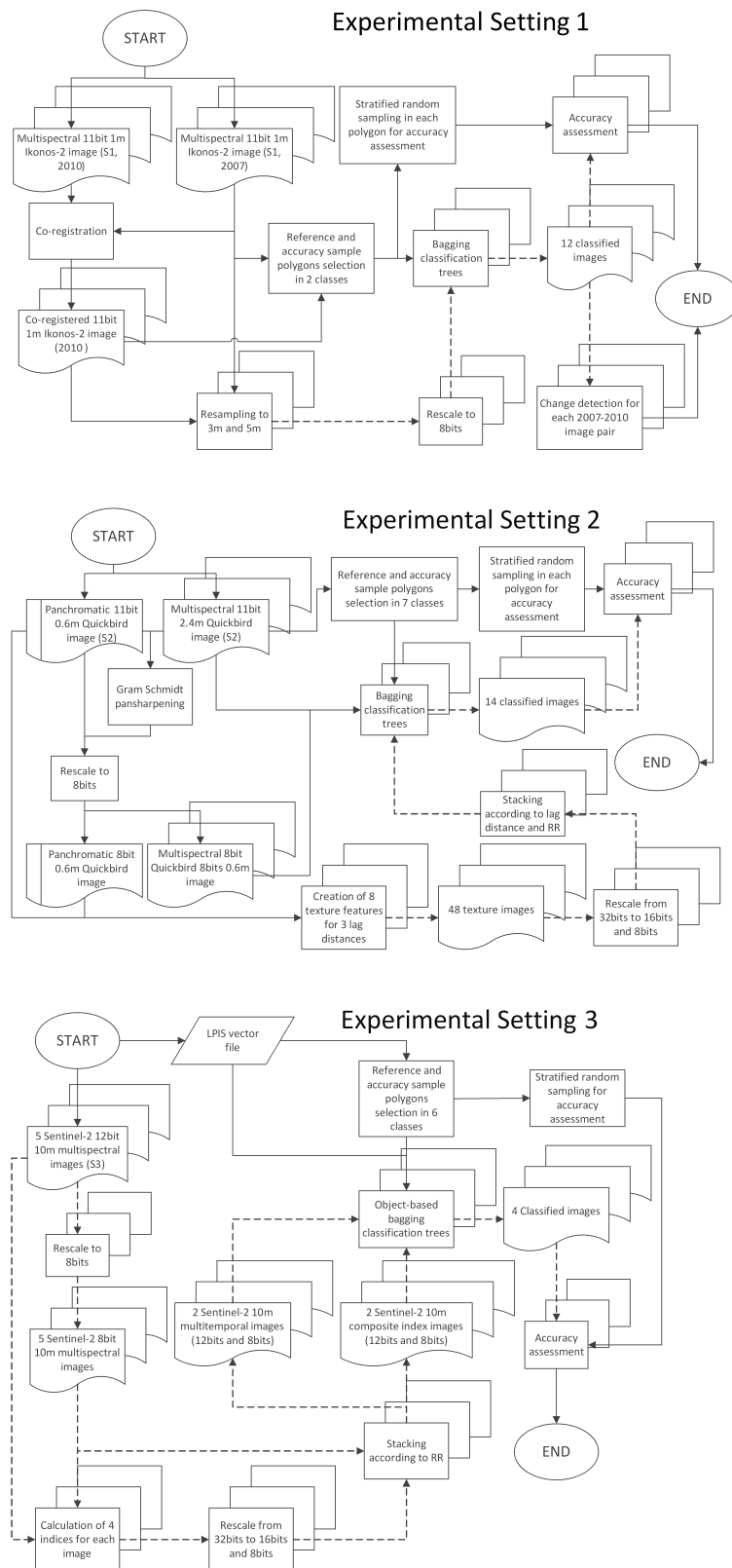


Figure 2. Overview of the three experimental designs.

2.5.1. Experimental Setting 1

Originally, the pansharpened Ikonos-2 image pair, was coregistered using a first order polynomial transformation with a total root mean square error of 0.57 pixels. A binary classification scheme (tile roofs/nontile roof areas) was adopted for evaluating impact of radiometric analysis on binary classification and change detection accuracy. Apart from the original resolution (1 m) of the pansharpened imagery, a nearest neighborhood resampling procedure was followed to further assess the impact of radiometric resolution over different spatial resolutions [38]. Accordingly, the 11-bit Ikonos-2 images were degraded to 3 m and 5 m spatial resolution that were subsequently rescaled to 8-bit resolution.

The reference data samples were manually selected based on visual interpretation of the Ikonos-2 images. Common reference areas of ‘no change’ in terms of roof cover, were digitized manually over the bitemporal set of the 1 m resolution images. Subsequently 1200 pixels were randomly selected within these areas and used for training the BCT classifier.

In this experiment, Ntree was set to 500, the optimal number of random variables to be tested in each tree (Mtry) was set to 4, (i.e., Ikonos-2 image bands), forcing the algorithm to use all the bands in order to avoid the ‘randomness’ of developing different models each time and minimize the influence of the spectral component in the classification accuracy.

In order to assess the accuracy of the results, validation pixels were selected using a stratified random sampling procedure within the reference polygons (excluding the polygons used in training procedure), selecting 10 points per polygon (244 points in total). Finally, overall accuracy (OA) and ‘kappa hat’ ($\hat{\kappa}$) values from each classification confusion matrix were derived.

2.5.2. Experimental Setting 2

The second experimental setting was designed in order to analyze the impact of radiometric resolution when employing a more detailed class scheme over a heterogeneous forest scene, representing a more demanding classification task compared to a binary one (experimental setting 1). Furthermore, since previous studies have indicated that texture features can improve classification accuracy in several tasks such as forest attributes estimation [39], or generic land cover classification [40], the effect of radiometry was examined in texture effectiveness for the accuracy improvement over the same scene and classification scheme. Texture can integrate additional information about spatial variance patterns, based on the assumption that a pixel is not independent of its neighbor pixels and that its dependence can be quantified and integrated into a classifier [41].

Initially, the bundle Quickbird image was pansharpened to 0.6 m using the Gram–Schmidt method which is one of the most accurate methods for better maintaining spectral (thus radiometric) characteristics of Quickbird data while improving spatial resolution [42]. Subsequently, the 11-bit pansharpened multispectral image was rescaled to 8 bits using the linear rescale method.

Five first-order texture measures (data range, mean, variance, entropy and skewness) and three local indicators of spatial association (LISA) (Moran’s I, Geary’s c and Geti’s G) were estimated from the panchromatic 0.6 m image, within various window sizes (5×5 , 15×15 and 25×25). Selection of the optimal window size or lag distance is a practical problem for texture quantification, which depends on the characteristics of the study area and the spatial resolution of the image and thus, may be different for each scene and classification task [40,43,44].

The texture classification was based on the panchromatic image instead of the multispectral one, in order to limit dataset size and avoid any bias related to spectral information content. A total of 24 texture synthetic bands (i.e., eight features and three window sizes each) were generated having a 32-bit resolution from the original 11-bit Quickbird panchromatic image. Furthermore, a set of 24 texture images were calculated after the radiometric degradation of the original 11-bit panchromatic image to an 8-bit one. Subsequently, these two texture datasets were rescaled again from 32 bits to 16 bits and 8 bits. The change from 32 bits to 16 bits was done because standard image formats store data in increments of 8 bits [45].

The resulting texture images were stacked together based on the respective window size, generating 12 image stacks in total.

Reference polygons have been previously delineated through ground surveys and visual delineation, where 190 plots have been accurately located via the gradsect method, using a GPS handheld device and printouts of the panchromatic image on a scale 1:2000 [44]. The classification scheme of experimental setting 2 was specified according to the forest vegetation within these plots, including seven classes: (1) beech, (2) oak, (3) conifers, (4) evergreen–oak species mix, (5) broadleaf–coniferous species mix, (6) grass, (7) bare ground.

For the BCT classification, a similar procedure with the previous experimental setting was followed: 3000 pixels were randomly selected within reference polygons and used for training. The quantities, *Ntree* and *Mtry*, were set to 500 and equal to the image stack bands, respectively. Finally, the accuracy assessment involved random selection of 10 points per polygon (excluding the polygons used as training).

2.5.3. Experimental Setting 3

The third experimental setting was designed in order to analyze the impact of the radiometric resolution when adopting objects as units of classification as well as in order to assess the impact of radiometric resolution in the information content and the discriminatory power of multiseasonal vegetation indices.

Prior to any processing, the three 60 m bands of Sentinel-2, primary designed for characterizing coastal areas, atmospheric aerosol, and thin cirrus clouds properties, were excluded from the image data sets. The remaining 10 m and 20 m bands were used in 10-band image stacks. Once again, the five Sentinel-2 images were rescaled from the original 12-bit to an 8-bit radiometric resolution. The 12-bit and 8-bit images were stacked generating 50-bands image stacks respectively.

Furthermore, since many studies employ spectral indices for quantifying relationships between seasonal remote sensing measurements and vegetation characteristics for limiting band correlation and data redundancy [26], four spectral indices were calculated from the multiseasonal Sentinel-2 original bands. The indices used included the Normalized Difference Vegetation Index (NDVI), the Normalized Difference Water Index (NDWI), the modified Normalized Difference Water Index (NDWI2), [46,47] and the Green Red Vegetation Index (GRVI) [26].

The 32-bit radiometric resolution indices were calculated from the original 12-bit and the rescaled 8-bit Sentinel-2 images. Subsequently, the four indices calculated for each month were stacked together, creating 20-bands stacks that were rescaled to 16-bit and 8-bit radiometric resolution datasets.

Similar to the previous experimental settings, a BCT classifier was employed albeit with a different unit of classification i.e., object. The availability over this rural area of a large-scale vector data-set, representing agricultural field entities (Land Parcel Identification System-LPIS), facilitated assessment of radiometric resolution impact on Geographic Object-Based Image Analysis (GEOBIA) classification process. Per-field or per-parcel image analysis [48] was adopted, a subtype of object-based approach, relying on the integration of remotely sensed imagery and existing vector maps that are used to define regions of contiguous pixels belonging to the same class.

Reference data selection in this experiment, relied on the thematic content of the LPIS spatial database of the area that included 15,054 field entities. Classification categories included wheat, rice, legumes, cotton, maize, and alfalfa fields. Ten percent of the fields per crop type were randomly selected from the LPIS dataset for training the BCT classifier (901 polygons) and another 10% for independent accuracy assessment. For the BCT classification, as in the previous settings, the quantities, *Ntree* and *Mtry*, were 500 and equal to the image stack bands, respectively.

3. Results

3.1. Experiment 1

Table 1 presents the OOB rate, the accuracy measures for the independent validation sample and the computational time needed for the twelve individual classification schemes included in the 1st experimental setting. In the case of the 1-m spatial resolution Ikonos image acquired in 2007, both 11-bit and 8-bit images presented the same overall accuracy (91%) and khat (0.82) values, however the 11-bit image classification procedure required 18% more computational time. In the case of the 2010 image classification, the use of the lower radiometric resolution resulted in slightly higher overall accuracy (OA = 88% and khat = 0.75), compared to the finer 11-bit radiometric resolution image (OA = 86% and khat = 0.72), with the former classification demanding also 10% less computational time.

Table 1. Accuracy assessment for the classifications of the pansharpened Ikonos images in experimental setting 1, using the training and testing samples.

Acquisition Year	Radiometric Resolution (bits)	Spatial Resolution (m)	OOB Error Rate (%)	Khat	Overall Accuracy (%)	Computational Time (s)
2007	11	1	6.33	0.82	91	94.74
2007	8	1	6.25	0.82	91	79.80
2007	11	3	6.25	0.78	89	62.15
2007	8	3	6.67	0.86	93	63.33
2007	11	5	6.33	0.75	88	61.96
2007	8	5	6.25	0.78	89	59.47
2010	11	1	8.00	0.72	86	93.46
2010	8	1	7.67	0.75	88	84.03
2010	11	3	5.50	0.75	88	61.83
2010	8	3	6.08	0.81	91	72.18
2010	11	5	8.17	0.78	89	61.09
2010	8	5	8.42	0.80	90	60.25

In the case of the spatially degraded images, while the OOB error rates suggested minor differences among the 11-bit and 8-bit classifications, the subsequent accuracy assessment using the independent validation samples, indicated that the use of the 8-bit imagery resulted in more accurate classification maps. The most profound changes are noted in the classification of the 8-bit, 3-m images, having 4% and 3% higher overall accuracy compared to 11-bit images, for the 2007 and 2010 datasets respectively. In terms of the computational cost, no significant differences are detected except for the case of the 2010 3-m, 8-bit image that required 17% more time than its 11-bit counterpart.

Visual assessment of the classification results showed minor differences among the two radiometric resolutions involved (Figure 3). Especially, in the case of the highest (1 m) spatial resolution datasets, noise (i.e., salt and pepper effect) is evident in the case of the lower radiometry image classification.

To evaluate the effect of radiometric resolution on change detection, the 8-bit change images were compared to the 11-bit change images in experimental setting 1. Accuracy metrics (Table 2), derived from the separate samples selected only for this evaluation, revealed very small differences between high/low radiometry change maps. Specifically, for the 1 m and 5 m images, overall accuracy had the same value in 8-bit and 11-bit images (86% and 82% accordingly), though khat improved by 2% (from 0.71 to 0.73 and 0.62 to 0.63 respectively) for the 11-bit images. On the other hand, the change map, based on the 3-m, 8-bit image pair, was slightly more accurate ($k = 0.75$, OA = 88%) than the respective map produced by 11-bit data ($k = 0.71$, OA = 85%). Visual assessment showed that the changed pixels from 2007 to 2010 appeared in the form of ‘noise’ in the 8-bit images. This phenomenon is closely related to the ‘salt and pepper’ effect of the single-date classifications, as mentioned earlier. Furthermore, the magnitude of change in each case was evaluated. As illustrated in Figure 4, in the case of the 11-bit images, pixels labeled with change are slightly more (19.9–25.5% of the area), than in the case of 8-bit images (18.3–22.2%), distributed across object boundaries.

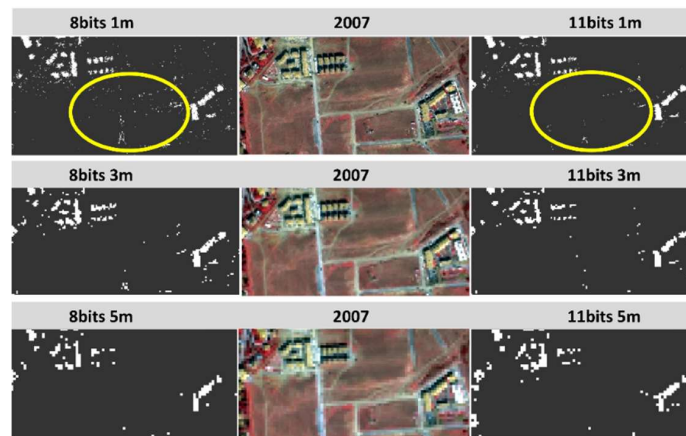


Figure 3. The ‘salt & pepper’ effect (yellow circle) observed within the lower radiometric resolution (8 bits) was evident in the high spatial resolution images (1 m). On the other hand, in lower spatial resolution images (3 m and 5 m) no differences were observed between low and high resolution radiometric datasets.

Table 2. Accuracy assessment for the 2007–2010 change detection of the classified Ikonos image pairs in experimental setting 1, using the testing samples.

Radiometric Resolution (bits)	Spatial Resolution (m)	Khat	Overall Accuracy (%)
16	1	0.73	86
8	1	0.71	86
16	3	0.71	85
8	3	0.75	88
16	5	0.63	82
8	5	0.62	82

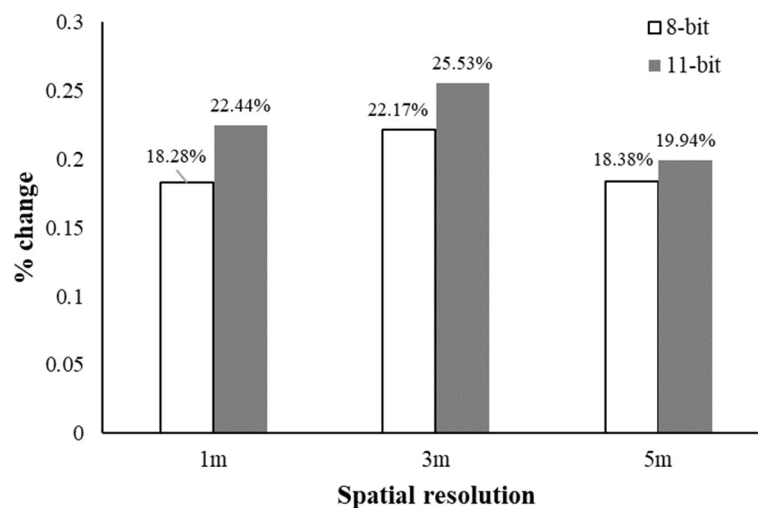


Figure 4. Comparison of change detection measurements using the high and low radiometric resolution images within the 1st experimental setting.

3.2. Experiment 2

As expected, the classification accuracy of the multiclass classifications over a diverse scene as in the 2nd experimental setting (Table 3), was lower compared to the accuracy figures resulting from the binary class scheme in the Triadi area. Classification of the pansharpened multispectral 11-bit image,

resulted in 68% overall accuracy (khat = 0.62), slightly higher than the degraded 8 bit image (OA = 67% and khat = 0.61).

Table 3. Accuracy assessment for the classifications of the pansharpened and synthetic (texture) Quickbird images in experimental setting 2, using the training and testing samples.

Dataset	Original Image Radiometry (bits)	Texture Radiometry (bits)	Window Size (p)	OOB Error Rate (%)	Khat	Overall Accuracy (%)	Computational Time (s)
Pansharpened MS	11	-	-	34.43	0.62	68	344.19
Pansharpened MS	8	-	-	35.67	0.61	67	340.27
Panchromatic	11	16	5	46.57	0.52	60	537.1
Panchromatic	11	8	5	26.93	0.59	66	467.26
Panchromatic	8	16	5	45.6	0.51	59	552.36
Panchromatic	8	8	5	47.97	0.44	54	510.27
Panchromatic	11	16	15	27.3	0.62	68	502.01
Panchromatic	11	8	15	29.27	0.59	66	476.69
Panchromatic	8	16	15	26.53	0.63	69	497.73
Panchromatic	8	8	15	29.47	0.58	65	469.38
Panchromatic	11	16	25	18.63	0.66	71	478.99
Panchromatic	11	8	25	19.53	0.63	69	460.47
Panchromatic	8	16	25	19.03	0.66	72	482.86
Panchromatic	8	8	25	20.17	0.63	69	460.79

In regard to the impact of the original image radiometry in the classification accuracy of texture bands, in all but in the 15×15 , 16-bit texture bands, the use of the lower radiometric 8-bit panchromatic image for estimating texture, generated similar or lower accuracies compared to the original 11-bit Quickbird data. The most profound differences were observed in the case of the smallest (i.e., 5×5 window), 8-bit texture bands, calculated upon the 8-bit Quickbird image, resulting to much lower accuracy (OA = 54%, khat = 0.44) compared to the accuracy of the 8-bit texture bands resulting from the 11-bit Quickbird image (OA = 66%, khat = 0.59).

Regarding the impact of the texture bands radiometry, the use of the 8-bit texture bands resulted in 3–7% lower classification accuracies, except for the case of the 11-bit Quickbird pan image, where the 8-bit, 5×5 window texture proved to be much more efficient (OA = 66%, khat = 0.59) than its 16-bit counterpart (OA = 60%, khat = 0.52).

The most accurate classifications were derived using the largest window size (i.e., 25×25), where the 16-bit texture bands of both the 11-bit and 8-bit Quickbird panchromatic images resulted in a khat value of 0.66. The khat values observed for the 5×5 and 15×15 bands were 0.59 and 0.63 respectively. Notably, in the case of the largest window size, individual classification differences among the various radiometry datasets were relatively lower (3% related to texture bands and 0% related to panchromatic image radiometry) compared to the 5×5 and 15×15 datasets.

For the second experimental setting, computational time difference between the 11-bit and 8-bit pansharpened multispectral datasets were negligible since the higher radiometric resolution required 1% more time for pixel assignment to classes. In the case of texture classification, the 11-bit panchromatic image was less time-demanding when either 16-bit or 8-bit texture bands (8% and 3% respectively) were employed compared to the 8-bit panchromatic image calculated upon the 5×5 window. The magnitude of respective differences was much smaller (i.e., approx. 1%) in the case of the 15×15 and 25×25 window size. The radiometry of the final texture bands had a higher impact on computational time since the 16-bit texture bands required up to 14.95% (3×3 window size, 11-bit panchromatic image) more time compared to the 8-bit stacks. In this case also, the use of larger window sizes minimized the impact of radiometry on time complexity.

3.3. Experiment 3

In the case of the multiseasonal object-based classifications, identical khat values (0.60) were obtained for the classification of the original bands either having 12-bit or 8-bit radiometry (Table 4).

Classification of the 16-bit spectral indices marginally (0.01) improved the khat values for the 12-bit or 8-bit Sentinel-2 images compared to the 8-bit spectral indices.

Table 4. Accuracy assessment for the classifications of the multiseasonal Sentinel-2 original and synthetic (indices) bands in experimental setting 3, using the training and testing samples.

Dataset	Original Image Radiometry (bits)	Spectral Indices Radiometry (bits)	OOB Error Rate (%)	Khat	Overall Accuracy (%)	Computational Time (s)
Original bands	12	-	23.40	0.60	78	17964.47
Original bands	8	-	23.84	0.60	77	17566.97
Spectral Indices	12	16	24.39	0.59	77	11535.23
Spectral Indices	12	8	23.95	0.58	78	11492.83
Spectral Indices	8	16	24.72	0.59	78	12412.53
Spectral Indices	8	8	25.28	0.58	77	12380.53

In terms of computational demand, while the original 12-bit bands required 2% more time compared to the 8-bit bands, in the case of spectral indices, the classifications of both the 8-bit and 16-bit stacks originating from the 12-bit Sentinel image were finished in 7% less time compared to the ones derived from the 8-bit Sentinel image. Almost no differences (less than 0.5%) were noted among 8-bit and 16-bit indices.

4. Discussion

The overall goal of this research was to assess the impact of radiometric resolution on image classification, adopting various classification schemes and considering different aspects of the classification road-map.

Except for one classification, the khat and overall accuracy metrics, indicated changes up to 8% related to the use of lower radiometric resolution. These results are consistent with many other studies that have been made on multispectral data [5,7–9,11], which report accuracy changes up to 8%. However, no relation was identified in the classification accuracy of different radiometric resolution images and spatial resolution change. In addition, it has been proven that spatial resolution can paradoxically be either beneficial or adverse to classification, depending on the land type being classified and that accuracy is dependent on class spectral variance, at different spatial scales [20,38].

Irons et al. [7], observed an increase in classification accuracy following degradation of spatial resolution (from 30 m to 80 m) in both 6-bit and 8-bit data, in a five-class scheme. Chen et al. [19], Pope & Rees [38], Roth et al. [20], compared classification accuracies of different spatial resolution data, while keeping the same radiometric resolution. In our case of the binary classification scheme we also noticed that the lower radiometric resolution resulted in higher classification accuracies (Table 1). This is likely related to the fact that the finer radiometric resolution, similar to spatial, leads to the detection of finer elements within the pixel. The detection of these components contributes to higher within-class variance, potentially contributing in lower accuracies.

The binary classification map of the 11-bit Ikonos data was less affected by salt and pepper classification noise than the 8-bit based map. Nevertheless, as spatial resolution decreased, the magnitude of the speckle was reduced.

In the case of texture classifications in the second experimental setting, accuracy results are marginally affected by radiometric resolution change, with texture window size playing the most important role in classification accuracy. The only exception was the large difference noted in the 8-bit texture stacks of 5×5 texture bands, produced by original 11-bit and the degraded 8-bit panchromatic images. As stated by Chen et al. [19], the optimum window size used for extracting texture features should be relatively larger in finer spatial resolutions, so the 5×5 window in the 0.6 m Quickbird image wasn't the best option for the landscape in the 2nd experiment. The rescale though, from 8-bits to 16-bits created a quantization to the image that imitated a larger window size, thus improving

classification accuracy. This observation is also coherent with classification accuracy increase when degrading spatial resolution [38]. To sum up, texture metrics are slightly affected by the radiometric resolution of the original satellite images.

Within the third experimental setting and the multiseasonal object-based classification considering the spectral indices, classification accuracy of the higher radiometric resolution spectral indices increased by 1%, indicating that spectral indices are barely affected by the radiometric resolution of the images from which they derive. This means that multiseasonal or even time-series analyses can rely on lower radiometry, thus saving computational time and space. These results are also supported by the results of Singh et al. [10], who found differences in K accuracies up to 6% when classifying NDVI images with 4-bit, 6-bit and 8-bit resolution images. This marginal increase of accuracy can also be observed when comparing quantities derived from indices of different radiometric resolution (such as LAI from NDVI) [6]. In addition to this, the per-field (object-based) approach of this experimental setting revealed that lower radiometric resolution data can be used safely in object-based classification. For the first experimental setting, between the 8-bit and 11-bit classified images, changes of around 10 sec (10–16%) for 1 m and 3 m spatial resolution were observed (Table 1). The magnitude of change was lower (1–4%) in the case of the 5 m spatial resolution data. Lower radiometric resolution image classification was usually more time efficient. In the third experimental setting (Table 4), the higher radiometric resolution images were more efficient in terms of time complexity (8%).

Image entropy was calculated for each band of the high and low radiometry satellite images, for image content assessment (Table 5). In general, little (less than 0.10%) or no differences were detected among high and low radiometry datasets. Hence, the difference in information content between high and low radiometric resolution data is negligible, considering that the improvement of the ETM+ sensor against the TM Landsat sensor in the recording information content was 1 bit/pixel [14]. This finding verifies the results of the classification accuracies, which showed that radiometric resolution reduction in the original data does not affect classification accuracy. Overall, our analysis over the three different classification experiments, demonstrates that the improvement in the classification inaccuracy from the higher radiometric detail is not that significant considering also the drawback of the increased data volume required for storing and processing such data. While the radiometric resolution impact on accuracy was assessed over a range of different classification settings we used a single machine learning classification algorithm. The use of a single algorithm (BCT) enabled us to focus more on the impact of the radiometric resolution, while minimizing the effects of parameters tuning and training sampling considerations [23]. New developments and more robust algorithms, such as the deep learning methods, might expand in the future the generalizability and transferability of our findings.

Table 5. Band entropy for the original multispectral images.

Dataset	Radiometric Resolution (bits)	Blue (B)	Green (G)	Red (R)	Red Edge (RE1)	Red Edge (RE2)	Near InfraRed Narrow 1 (NIRn1)	Near InfraRed (NIR)	Near InfraRed Narrow 2 (NIRn2)	ShortWave InfraRed (SWIR1)	ShortWave InfraRed (SWIR2)
Ikonos-2007	11	19.88	19.87	19.84	-	-	-	19.86	-	-	-
Ikonos-2007	8	19.86	19.86	19.84	-	-	-	19.85	-	-	-
Difference (%)		0.10	0.05	0.00				0.05			
Ikonos-2010	11	19.83	19.81	19.75	-	-	-	19.83	-	-	-
Ikonos-2010	8	19.83	19.81	19.75	-	-	-	19.83	-	-	-
Difference (%)		0.00	0.00	0.00				0.00			
Quickbird	11	23.55	23.55	23.52	-	-	-	23.52	-	-	-
Quickbird	8	23.53	23.55	23.52	-	-	-	23.52	-	-	-
Difference (%)		0.08	0.00	0.00				0.00			
S2-March 2017	12	23.51	23.53	23.36	23.44	23.4	23.38	23.38	23.38	23.4	23.35
S2-March 2017	8	23.51	23.53	23.36	23.44	23.4	23.38	23.38	23.38	23.4	23.35
Difference (%)		0.00	0.00	0.00	0.00	0.00	0.00	0.00	0.00	0.00	0.00
S2-May 2017	12	23.51	23.56	23.47	23.55	23.47	23.45	23.43	23.43	23.37	23.33
S2-May 2017	8	23.51	23.56	23.47	23.55	23.47	23.45	23.43	23.43	23.37	23.33
Difference (%)		0.00	0.00	0.00	0.00	0.00	0.00	0.00	0.00	0.00	0.00
S2-June 2017	12	23.34	23.47	23.23	23.47	23.48	23.46	23.46	23.46	23.46	23.41
S2-June 2017	8	23.33	23.47	23.23	23.47	23.48	23.46	23.46	23.46	23.46	23.4
Difference (%)		0.04	0.00	0.00	0.00	0.00	0.00	0.00	0.00	0.00	0.04
S2-July 2017	12	23.28	23.44	23.12	23.45	23.46	23.43	23.43	23.43	23.47	23.39
S2-July 2017	8	23.27	23.44	23.12	23.45	23.46	23.43	23.43	23.43	23.47	23.39
Difference (%)		0.04	0.00	0.00	0.00	0.00	0.00	0.00	0.00	0.00	0.00
S2-August 2017	12	23.42	23.48	23.20	23.41	23.39	23.37	23.37	23.38	23.39	23.3
S2-August 2017	8	23.42	23.48	23.21	23.41	23.39	23.37	23.37	23.38	23.38	23.29
Difference (%)		0.00	0.00	-0.04	0.00	0.00	0.00	0.00	0.00	0.04	0.04

5. Conclusions

The role of radiometric resolution on classification accuracy, as well as on image information content and computational complexity was experimentally assessed in this study. The key findings indicate the low impact of radiometric resolution in classification accuracy, at least in the experiments included in this study. In the case of texture classification, the different experiments also indicated differences in classification accuracies up to 7% except from one case. In object-based classification of the multiseasonal spectral indices, classification accuracy difference between higher and lower radiometric resolution datasets were much lower (1%) compared to pixel-based experiments.

Higher radiometric resolution did not appear to have a significant effect on BCT classification times, except for the object-based approach.

Entropy analysis of the original images for each study area, for the initial and degraded radiometric resolution, showed differences that did not exceed 0.02 bits/pixel. This implies that the difference in information content in the high and low radiometric resolution data is negligible.

This research suggests some hints on selecting or modifying radiometric resolution for certain classification tasks, as it provides indications that lower radiometric resolution is not always at the expense of classification accuracy.

Future research could address more deeply the interrelations between radiometric and other types of remote sensing resolutions as well as the impact of the classification algorithm used in the classification accuracy of various radiometric resolution images.

Author Contributions: G.M. and M.T.-S. conceived the idea and developed the research design. N.V. implemented the analysis. N.V. and G.M. wrote and edited the manuscript. M.T.-S., P.P. and C.G. contributed in the interpretation of the results and provided feedback on the manuscript during its initial preparation and revision.

Funding: This research received no external funding.

Acknowledgments: Sentinel 2 MSI data used were available at no cost from ESA Sentinels Scientific Data Hub. Quickbird data acquisition was supported by the Greek General Secretariat for Research and Technology, in the framework of the Operational Programme “Competitiveness”.

Conflicts of Interest: The authors declare no conflict of interest.

References

1. Thenkabail, P.S. (Ed.) *Remote Sensing Handbook. Volume I, Remotely Sensed Data Characterization, Classification, and Accuracies*; CRC Press: Boca Raton, FL, USA, 2015; ISBN 9781482217865.
2. Ma, Y.; Wu, H.; Wang, L.; Huang, B.; Ranjan, R.; Zomaya, A.; Jie, W. Remote sensing big data computing: Challenges and opportunities. *Future Gener. Comput. Syst.* **2015**, *51*, 47–60. [[CrossRef](#)]
3. Serra-Sagrístà, J.; Aulí-Llinàs, F. Remote Sensing Data Compression. *Comput. Intell. Remote Sens.* **2008**, 27–61. [[CrossRef](#)]
4. Benediktsson, J.A.; Chanussot, J.; Moon, W.M. Very High-Resolution Remote Sensing: Challenges and Opportunities [Point of View]. *Proc. IEEE* **2012**, *100*, 1907–1910. [[CrossRef](#)]
5. Tucker, C.J. Radiometric resolution for monitoring vegetation How many bits are needed? *Int. J. Remote Sens.* **1980**, *1*, 241–254. [[CrossRef](#)]
6. Rao, N.; Garg, P.; Ghosh, S. The Effect of Radiometric Resolution on the Retrieval of Leaf Area Index from Agricultural Crops. *GISci. Remote Sens.* **2006**, *43*, 377–387. [[CrossRef](#)]
7. Irons, J.R.; Markham, B.L.; Nelson, R.F.; Toll, D.L.; Williams, D.L.; Latty, R.S.; Stauffer, M.L. The effects of spatial resolution on the classification of Thematic Mapper data. *Int. J. Remote Sens.* **1985**, *6*, 1385–1403. [[CrossRef](#)]
8. Legleiter, C.J.; Marcus, A.; Lawrence, R.L. Effects of Sensor Resolution on Mapping In-Stream Habitats. *Photogramm. Eng. Remote Sens.* **2002**, *68*, 801–807.
9. Platt, R.; Goetz, A. A comparison of AVIRIS and synthetic Landsat data for land use classification at the urban fringe. *Photogramm. Eng. Remote Sens.* **2004**, *70*, 813–819. [[CrossRef](#)]

10. Singh, R.P.; Dadhwal, V.K.; Singh, K.P.; Navalgund, R.R. Study on sensor's spatial, radiometric and temporal resolution requirements for crop monitoring. In Proceedings of the Symposium on Advances in Electronics, ELECTRO-2001, Varanasi, India, 4–6 January 2001; pp. 4–6.
11. Rama Rao, N.; Garg, P.K.; Ghosh, S.K. Evaluation of radiometric resolution on land use/land cover mapping in an agricultural area. *Int. J. Remote Sens.* **2007**, *28*, 443–450. [[CrossRef](#)]
12. Bernstein, R.; Lotspiech, J.B.; Myers, H.J.; Kolsky, H.G.; Lees, R.D. Analysis and Processing of LANDSAT-4 Sensor Data Using Advanced Image Processing Techniques and Technologies. *IEEE Trans. Geosci. Remote Sens.* **1984**, *GE-22*, 192–221. [[CrossRef](#)]
13. Malila, W.A. Comparison of the Information Contents of Landsat TM and MSS Data. *Photogramm. Eng. Remote Sens.* **1985**, *51*, 1449–1457.
14. Masek, J.G.; Honzak, M.; Goward, S.N.; Liu, P.; Pak, E. Landsat-7 ETM+ as an observatory for land cover initial radiometric and geometric comparisons with Landsat-5 Thematic Mapper. *Remote Sens. Environ.* **2001**, *78*, 118–130. [[CrossRef](#)]
15. Karnieli, A.; Ben-Dor, E.; Bayarjargal, Y.; Lugasi, R. Radiometric saturation of Landsat-7 ETM+ data over the Negev Desert (Israel): Problems and solutions. *Int. J. Appl. Earth Obs. Geoinf.* **2004**, *5*, 219–237. [[CrossRef](#)]
16. Alonso, C.; Tarquis, A.M.; Zúñiga, I.; Benito, R.M. Spatial and radiometric characterization of multi spectrum satellite images through multi-fractal analysis. *Nonlinear Process. Geophys.* **2017**, *24*, 141–155. [[CrossRef](#)]
17. Elmore, A.J.; Mustard, J.F. Precision and accuracy of EO-1 Advanced Land Imager (ALI) data for semiarid vegetation studies. *IEEE Trans. Geosci. Remote Sens.* **2003**, *41*, 1311–1320. [[CrossRef](#)]
18. Orych, A.; Walczykowski, P.; Jenerowicz, A.; Zdunek, Z. Impact of the cameras radiometric resolution on the accuracy of determining spectral reflectance coefficients. *Int. Arch. Photogramm. Remote Sens. Spat. Inf. Sci. ISPRS Arch.* **2014**, *40*, 347–349. [[CrossRef](#)]
19. Chen, D.; Stow, D.A.; Gong, P. Examining the effect of spatial resolution and texture window size on classification accuracy: An urban environment case. *Int. J. Remote Sens.* **2004**, *25*, 2177–2192. [[CrossRef](#)]
20. Roth, K.L.; Roberts, D.A.; Dennison, P.E.; Peterson, S.H.; Alonzo, M. The impact of spatial resolution on the classification of plant species and functional types within imaging spectrometer data. *Remote Sens. Environ.* **2015**, *171*, 45–57. [[CrossRef](#)]
21. Herold, M.; Gardner, M.E.; Roberts, D.A. Spectral resolution requirements for mapping urban areas. *IEEE Trans. Geosci. Remote Sens.* **2003**, *41*, 1907–1919. [[CrossRef](#)]
22. Dalponte, M.; Bruzzone, L.; Vescovo, L.; Gianelle, D. The role of spectral resolution and classifier complexity in the analysis of hyperspectral images of forest areas. *Remote Sens. Environ.* **2009**, *113*, 2345–2355. [[CrossRef](#)]
23. Maxwell, A.E.; Warner, T.A.; Fang, F. Implementation of machine-learning classification in remote sensing: An applied review. *Int. J. Remote Sens.* **2018**, *39*, 2784–2817. [[CrossRef](#)]
24. Berger, M.; Moreno, J.; Johannessen, J.A.; Levelt, P.F.; Hanssen, R.F. ESA's sentinel missions in support of Earth system science. *Remote Sens. Environ.* **2012**, *120*, 84–90. [[CrossRef](#)]
25. Gascon, F.; Bouzinac, C.; Thépaut, O.; Jung, M.; Francesconi, B.; Louis, J.; Lonjou, V.; Lafrance, B.; Massera, S.; Gaudel-Vacaresse, A.; et al. Copernicus Sentinel-2A calibration and products validation status. *Remote Sens.* **2017**, *9*, 584. [[CrossRef](#)]
26. Siachalou, S.; Mallinis, G.; Tsakiri-Strati, M. Analysis of Time-Series Spectral Index Data to Enhance Crop Identification Over a Mediterranean Rural Landscape. *IEEE Geosci. Remote Sens. Lett.* **2017**, 1–5. [[CrossRef](#)]
27. Breiman, L. Bagging predictors. *Mach. Learn.* **1996**, *24*, 123–140. [[CrossRef](#)]
28. Belgiu, M.; Drăgu, L.; Drăguț, L. Random forest in remote sensing: A review of applications and future directions. *ISPRS J. Photogramm. Remote Sens.* **2016**, *114*, 24–31. [[CrossRef](#)]
29. Liaw, A.; Wiener, M. Classification and Regression by randomForest. *R News* **2002**, *2*, 18–22. [[CrossRef](#)]
30. R Core Team. *R: A Language and Environment for Statistical Computing*; R Core Team: Vienna, Austria, 2017.
31. Chrysafis, I.; Mallinis, G.; Gitas, I.; Tsakiri-Strati, M. Estimating Mediterranean forest parameters using multi seasonal Landsat 8 OLI imagery and an ensemble learning method. *Remote Sens. Environ.* **2017**, *199*, 154–166. [[CrossRef](#)]
32. Congalton, R.G. A review of assessing the accuracy of classifications of remotely sensed data. *Remote Sens. Environ.* **1991**, *37*, 35–46. [[CrossRef](#)]
33. Foody, G.M. Status of land cover classification accuracy assessment. *Remote Sens. Environ.* **2002**, *80*, 185–201. [[CrossRef](#)]

34. Katiyar, S.; Arun, P. A Review Over the Applicability of Image Entropy in Analyses of Remote Sensing Datasets. *arXiv* 2014, arXiv:1405.6133. Available online: <https://arxiv.org/ftp/arxiv/papers/1405/1405.6133.pdf> (accessed on 11 August 2018).
35. Healey, S.P.; Cohen, W.B.; Zhiqiang, Y.; Krankina, O.N. Comparison of Tasseled Cap-based Landsat data structures for use in forest disturbance detection. *Remote Sens. Environ.* **2005**, *97*, 301–310. [[CrossRef](#)]
36. Hausser, J.; Strimmer, K. Entropy: Estimation of Entropy, Mutual Information and Related Quantities 2014. Available online: <https://cran.r-project.org/web/packages/entropy/index.html> (accessed on 11 August 2018).
37. Franks, S. How Many Bits? Radiometric Resolution as a Factor in Obtaining Forestry Information with Remotely Sensed Measurements. Master's Thesis, University of Maryland, College Park, MD, USA, 2006.
38. Pope, A.; Rees, W.G. Impact of spatial, spectral, and radiometric properties of multispectral imagers on glacier surface classification. *Remote Sens. Environ.* **2014**, *141*, 1–13. [[CrossRef](#)]
39. Dube, T.; Mutanga, O. Investigating the robustness of the new Landsat-8 Operational Land Imager derived texture metrics in estimating plantation forest aboveground biomass in resource constrained areas. *ISPRS J. Photogramm. Remote Sens.* **2015**, *108*, 12–32. [[CrossRef](#)]
40. Rodriguez-Galiano, V.F.; Chica-Olmo, M.; Abarca-Hernandez, F.; Atkinson, P.M.; Jeganathan, C. Random Forest classification of Mediterranean land cover using multi-seasonal imagery and multi-seasonal texture. *Remote Sens. Environ.* **2012**, *121*, 93–107. [[CrossRef](#)]
41. Chica-Olmo, M.; Abarca-Hernández, F. Computing geostatistical image texture for remotely sensed data classification. *Comput. Geosci.* **2000**, *26*, 373–383. [[CrossRef](#)]
42. Sarp, G. Spectral and spatial quality analysis of pan-sharpening algorithms: A case study in Istanbul. *Eur. J. Remote Sens.* **2014**, *47*, 19–28. [[CrossRef](#)]
43. Wang, H.; Zhao, Y.; Pu, R.; Zhang, Z. Mapping Robinia Pseudoacacia Forest Health Conditions by Using Combined Spectral, Spatial, and Textural Information Extracted from IKONOS Imagery and Random Forest Classifier. *Remote Sens.* **2015**, *7*, 9020–9044. [[CrossRef](#)]
44. Mallinis, G.; Koutsias, N.; Tsakiri-Strati, M.; Karteris, M. Object-based classification using Quickbird imagery for delineating forest vegetation polygons in a Mediterranean test site. *ISPRS J. Photogramm. Remote Sens.* **2008**, *63*, 237–250. [[CrossRef](#)]
45. Navulur, K. Radiometric Resolution. In *Multispectral Image Analysis Using the Object-Oriented Paradigm*; CRC Press/Taylor & Francis: Boca Raton, FL, USA, 2007; pp. 10–11. ISBN 9781420043068.
46. Xiao, X.; Boles, S.; Frolking, S.; Li, C.; Babu, J.Y.; Salas, W.; Moore, B. Mapping paddy rice agriculture in South and Southeast Asia using multi-temporal MODIS images. *Remote Sens. Environ.* **2006**, *100*, 95–113. [[CrossRef](#)]
47. Zhang, T.; Su, J.; Liu, C.; Chen, W. Band Selection in Sentinel-2 Satellite for Agriculture Applications. In Proceedings of the 23rd International Conference on Automation and Computing (ICAC), Huddersfield, UK, 7–8 September 2017; pp. 7–8.
48. Aplin, P.; Atkinson, P.M.; Curran, P.J. Fine spatial resolution simulated satellite sensor imagery for land cover mapping in the United Kingdom. *Remote Sens. Environ.* **1999**, *68*, 206–216. [[CrossRef](#)]

